

Topological and Thermoelectric Properties of Double Antiperovskite Pnictides

Wen Fong Goh and Warren E. Pickett

Department of Physics, University of California Davis 95616 CA, USA

(Dated: November 21, 2021)

Doubling the perovskite cell (double perovskite) has been found to open new possibilities for engineering functional materials, magnetic materials in particular. This route should be applicable to the antiperovskite (aPV) class. In the pnictide based double aPV (2aPV) class introduced here magnetism is very rare, and we address them as new topological materials, possibly with thermoelectric interest. We have found that the 2aPV supercell provides a systematically larger band gap that can serve to inhibit bulk conductivity, and also large spin-orbit coupling (SOC) for band inversion. We present examples from a broad study of double antiperovskites focusing on the $X_6AA'B_2$ configuration, where X is the alkaline earth element and A and B are the group 5A pnictogens. We find that an “extended s” state at the valence band minimum, described alternatively as a cation valence state or a modulated interstitial planewave state, plays a crucial role in both topological and thermoelectric properties. Several of these compounds may house topological phases, while transport calculations indicate they may also find themselves useful in thermoelectric applications.

PACS numbers:

I. INTRODUCTION

In spite of many existing classes of proposed topological insulators (TIs), the search for new classes with more favorable properties continues. One important factor is that most existing TIs are defective in the interior, thus are not insulating enough in the bulk to allow study and potential application of their surface bands. One recipe for finding new TIs is to look for small gap insulators that have valence and conduction bands with opposite parity and with small or negative gaps, and a different chemistry that might promote stoichiometry. For very small gap materials, the bands may be inverted by spin orbit-coupling (SOC), leading to insulating gaps that house topological states.¹ Ideally, the band gap (without SOC) must be small enough for band inversion, while large enough to inhibit bulk conductivity and enable application at room temperature. The other possibility is to have a band overlap semimetal (before SOC), with a gap opened at the Fermi level by SOC. In both cases the strength of SOC governs the magnitude of gap that can be obtained. This realization has focused attention on heavy atoms with large SOC.

Thermoelectric properties, based foremost on a large Seebeck coefficient, also in essence require small band gaps, since one wants a large derivative of the electronic density of states at the Fermi level, $dN(E)/dE|_{E_F}$, with strong particle-hole asymmetry and a low carrier density to minimize electronic thermal conduction. Unlike topological properties which depend sensitively to the momentum \vec{k} dispersion of bands on either side of the gap, for thermoelectric properties the energy dependence $[N(E)$, and the square velocity $v^2(E)$ of carriers at energy E] is the focus. At this level of discussion any connection between topological and thermoelectric properties not evident, aside from the importance of a small or possibly zero gap.

Compounds containing heavy atoms become of special interest. First, if gapped, the gap often is small, favorable for both thermoelectric and topological properties. Of course SOC is large, increasing the likelihood of band inversion and topological character. However, a connection, though somewhat indirect, has been predicted and demonstrated by Singh and collaborators.^{2,3} The key variable is the strength of SOC, which is large for heavy atoms, and the observation that in highly itinerant materials this strength can be varied quasi-continuously by isovalent doping. Substituting, say, Te with Se decreases the SOC strength, thereby tuning the band structure near the gap and adjusting both topological and thermoelectric properties. The predicted effect was verified by contrasting Bi_2Te_3 with isostructural and isovalent $\text{Bi}_2\text{Te}_2\text{Se}$.³

As just pointed out, heavy elements such as bismuth (Bi) and tellurium (Te) are favorable for TIs. A handful of materials, viz. Bi_2Se_3 family⁴⁻⁶ and Bi- and Te-based perovskites,^{7,8} have been discovered to possess non-trivial topological characteristics. Perovskites, primarily oxide-based ones, are one of the more prevalent structures to be explored and designed, due to their cubic structure and multitude of members. Their electronic structures often display a narrow gap with band minimum and maximum at high symmetry points,⁹⁻¹¹ implying that these materials may have potential in thermoelectric applications.¹² Doubling the structures will affect the dispersion and have been suggested in certain cases to increase the topological insulator’s bulk energy gap.^{13,14}

In this paper, we study the topological nature and the electronic structure based thermoelectric properties of several pnictide-based double antiperovskites, based on our previous study on single antiperovskite compounds¹⁵. Our methods of calculations are described in Sec. II, followed in Sec. III by a description of the structures. In Sec. IV the calculated band gaps and inversion energies are provided for the $X_6AA'B_2$ class of compounds, where

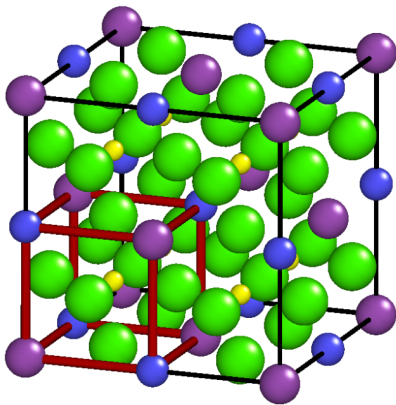


FIG. 1: Crystal structure of a double antiperovskite with A (purple) $\neq A'$ (blue) and $B = B'$ (small yellow spheres). Cations (green) form octahedra surrounding the B anions.

X is one of the divalent alkaline earths Ca, Sr, and Ba; AA' are pairs of heavy pnictides SbAs, BiAs, and BiSb; B is one of the lighter pnictides N, P, and As. The electronic structures of two of the compounds are illustrated in Sec. IV. In Sec. V the possibilities for topological properties are outlined, including effects of uniaxial strain. The thermoelectric coefficients of two illustrative compounds are presented in Sec. VI, and Sec. VII provides a brief summary.

II. METHODS

The electronic structure calculations are done with the full-potential local orbital (FPLO) code¹⁶, using the generalized gradient approximation (GGA) exchange-correlation of Perdew, Burke, and Ernzerhof¹⁷. A dense $20 \times 20 \times 20$ k -mesh was used for self-consistency because of the delicate band overlap near Γ . Spin-orbit coupling (SOC), in fact all relativistic effects, was included precisely by using the fully relativistic four component Kohn-Sham-Dirac equation implemented in FPLO, without resorting to the customary intermediate scalar relativistic approximation.

The calculations of thermoelectric properties are done in BoltzTraP¹⁹ by solving the Boltzmann equation via band interpolation scheme based on the band energy obtained from WIEN2k calculation¹⁸. A dense k -point mesh of 125000 (3107 in IBZ) are used and interpolated onto a mesh of 20 times denser. Bands within 4 eV around the Fermi level are used in the integration, with a fine energy mesh of 0.5 meV.

III. CRYSTAL STRUCTURE

The fcc double antiperovskite structure in Fig. 1 contains two alternating unit cells of a single antiperovskite

cube, denoted in generality by $X_6AA'BB'$, where X is an alkaline earth element and A, A', B, B' are pnictide elements on the A and B sites of the perovskite structure. Since the B and B' anions are surrounded by X_6 octahedra, if $B \neq B'$ then X is not required by symmetry to lie midway between them. However, $A \neq A'$ but $B = B'$, X does still reside on the special site midway between X ions. With distinct A -site atoms but $B = B'$, the spacegroup is $Fm\bar{3}m$ (#225). Both A and A' have a site symmetry of $m\bar{3}m$, while B and X have a site symmetry of $\bar{4}3m$ and mmm respectively. The optimized lattice constants of the double aPVs are close to twice of that of the single aPVs.

We are interested in $A \neq A'$ and $B = B'$ because the A site pnictide provides the upper valence bands at the gap (or band overlap). Thus modulation on the A site is of particular interest. Based on our previous study on the topological characteristics of antiperovskites, 21 double antiperovskites $X_6AA'B_2$ involving heavy elements, where $X = \text{Ca, Sr, Ba}$, $A = \text{Sb or Bi}$, $A' = \text{Sb or As}$, and $B = \text{N, P, and As}$, were selected for the study of potential topological characteristics.

IV. ELECTRONIC STRUCTURE

Near the gap (or band overlap) at Γ , which is the region of interest, these antiperovskites have valence bands contributed from the A site pnictide anion p bands, while the conduction bands derive from the alkaline-earth cation d bands. Doubling to $B - B'$ pairs leaves the direct (positive or negative) gap at the Γ point, with examples shown in Fig. 2. Studying the eigenvalues at the Γ point then gives an idea of which candidates are most likely to be topological insulators.

As pointed out previously,¹⁵ the bands disperse quadratically from Γ except for a single high velocity band which can become nearly linear if it approaches a valence band with small or negative gap, a peculiarity of this antiperovskite structure. From the projected density of states (DOS) this unusual band has even parity s -character on both cation and anion sites, so we refer to this band as an extended s -like state (ext- S). Since this ext- S character has opposite parity to the occupied bands, inverting it with the odd parity valence band maximum state at the Γ point transforms the system into a topological state.

A convenient way to determine if the system is in a topological insulating state is by looking at the band ordering at Γ , since band orderings at the other time reversal invariant momenta (high symmetry zone edge points) are widely gapped and never change in these systems. It is common, especially with heavy atoms, that SOC closes the band gap and inverts the band ordering. The band structure of $\text{Ca}_6\text{BiAsP}_2$ with SOC shown in Fig. 2b depicts a zero gap semiconducting state. At Γ the band at the Fermi level has a two-fold degeneracy (excluding spin degeneracy) and pushes the even parity ext- S -state

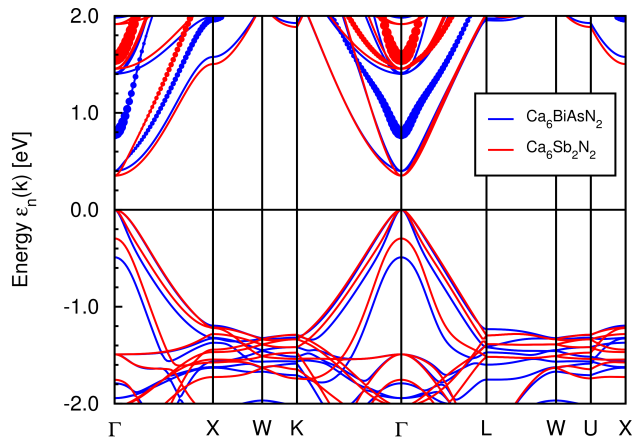
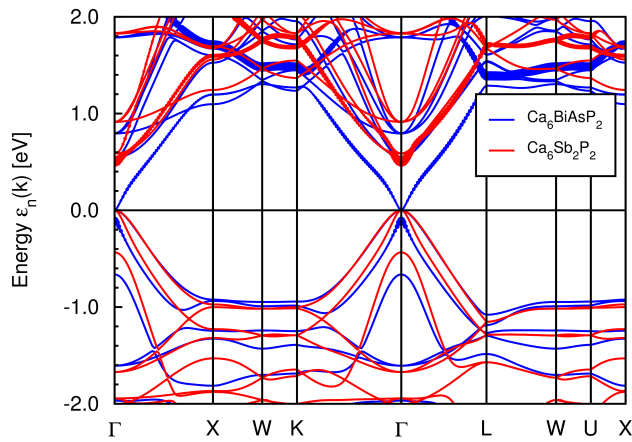
(a) $\text{Ca}_6\text{BiAsN}_2$ vs $\text{Ca}_6\text{Sb}_2\text{N}_2$.(b) $\text{Ca}_6\text{BiAsP}_2$ vs $\text{Ca}_6\text{Sb}_2\text{P}_2$.

FIG. 2: Band structure of double antiperovskites, to compare and contrast $\text{Ca}_6\text{BiAsN}_2$ and $\text{Ca}_6\text{Sb}_2\text{N}_2$ (above), and $\text{Ca}_6\text{BiAsP}_2$ and $\text{Ca}_6\text{Sb}_2\text{P}_2$ (below). Spin-orbit coupling included in all plots. The fat bands show even parity s -character of the heavy A atoms (As, Sb, Bi).

into the occupied region. This band inversion leaves a topological zero-gap insulating state, with a Z_2 invariant of 1;(000).

It is instructive to compare the electronic structure of double antiperovskites to a reference single antiperovskites in double perovskite supercell structure, especially when the reference has a B atom that is midway between the two in the double aPV. In Fig. 2, where SOC is included, the band gaps of $\text{Ca}_6\text{BiAsN}_2$ and $\text{Ca}_6\text{Sb}_2\text{N}_2$ are equal. Changing the cation to Sr gives a different result: $\text{Sr}_6\text{BiAsN}_2$ is a zero gap semiconductor while $\text{Sr}_6\text{Sb}_2\text{N}_2$ has about 0.5 eV energy gap. The former is a topological

zero gap semiconductor, the latter is a trivial semiconductor. The difference is the position of the ext- S state at Γ . The difference does however indicate that double aPVs are more likely to undergo band inversion than single aPVs.

We have surveyed the isovalent class of Ae-Pn double aPV compounds. Changing the B atom to a heavier one, for example, from $\text{Ca}_6\text{BiAsN}_2$ to $\text{Ca}_6\text{BiAsP}_2$ lowers the position of the ext- S band, giving smaller inversion energy and more likely topological character (see Table I). Similar conclusions result when changing the size of A and A' atoms, although sometimes the volume change affects this trend. In summary, heavy elements favor band inversion but volume effects are relevant. There are cases for which the band inversion can arise without the help of SOC. For example, in $\text{Sr}_6\text{BiAsP}_2$ where the interplay of element size and volume of the system has reached the ideal point, band inversion occurs without SOC.

V. TOPOLOGICAL STATES

The inversion energy is defined as the eigenvalue of the even ext- S -state minus that of the odd valence band p-state, thus negative inversion energies will promote a non-trivial Z_2 index. From Table I, $\{\text{Ca}, \text{Sr}, \text{Ba}\}_6\text{BiAsP}_2$, $\text{Sr}_6\text{BiSbP}_2$ and $\{\text{Ca}, \text{Sr}, \text{Ba}\}_6\text{BiSbAs}_2$ show negative inversion energy. Since band calculations with GGA exchange-correlation often underestimate the experimental band gap and give spurious inversion results, it is common to include the modified Becke-Johnson (mBJ) exchange-correlation potential^{20–22}, which provides a self-energy-like correction to the eigenvalues. On average, the GGA inversion energy is in the range of 0.3 eV while mBJ splits the valence and conduction bands by about 0.7 eV. This increase in gap is detrimental in obtaining topological states.

However, strain can open up a gap by symmetry-allowed hybridization, while promoting the inverted band ordering with non-trivial topological invariant. Without SOC, for example, (001) strain splits the p triplet at Γ into a singlet and a doublet, with one *rising* in energy (narrowing the gap or inverting the bands) and the other being lowered, depending on the sign of strain. Similarly, SOC splits the doublet, with the eigenvalue that is displaced upward tending to decrease or invert the gap. For $\text{Ca}_6\text{BiAsP}_2$ for example, the maximum gap achieved is 70 meV with compressive strain of 6%, but 110 meV in $\text{Sr}_6\text{BiAsP}_2$ with compressive strain of 8%. Fig. 3 shows the band structures of 5% compressive and tensile strain.

Both signs of strain result in topological states. Due to the band inversion at the Γ point for the compressive case, the Z_2 invariant is [1;000], a strong topological insulator state results. The topological surface bands crossing within the bulk band gap will give rise to a Dirac point. Tensile strain, on the other hand, produces a Dirac semimetal, with bands gapped everywhere except near Γ along Γ -Z, thus two symmetry related Dirac points. The

TABLE I: This table provides the effect of mBJ gap correction to the GGA+SOC band energies, for the inversion energy (see text) and the band gap, of selected double antiperovskites. Results are presented for B site pnictogen smaller than the A, A' atoms, because these are the only energetically stable combinations.

X ₆ AA'B ₂		B	N			P			As		
AA'	X		SOC	SOC+mBJ	mBJ effect	SOC	SOC+mBJ	mBJ effect	SOC	SOC+mBJ	mBJ effect
SbAs	Ca	Inversion Energy	1.28	2.39	1.11	0.30	1.08	0.78			
		Band Gap	0.51	1.15	0.64	0.30	1.08	0.78			
	Sr	Inversion Energy	0.63	1.71	1.08	0.03	0.82	0.78			
		Band Gap	0.38	1.03	0.66	0.03	0.82	0.78			
	Ba	Inversion Energy	0.49	1.45	0.96	0.15	0.92	0.77			
		Band Gap	0	0.53	0.53	0.15	0.85	0.70			
BiAs	Ca	Inversion Energy	0.82	1.92	1.10	-0.07	0.69	0.76			
		Band Gap	0.40	1.05	0.65	0	0.69	0.69			
	Sr	Inversion Energy	0.29	1.36	1.07	-0.29	0.48	0.76			
		Band Gap	0.29	1.00	0.70	0	0.48	0.48			
	Ba	Inversion Energy	0.31	1.29	0.97	-0.12	0.63	0.75			
		Band Gap	0	0.56	0.56	0	0.63	0.63			
BiSb	Ca	Inversion Energy	1.07	2.09	1.02	0.10	0.84	0.74	-0.17	0.56	0.73
		Band Gap	0.21	0.81	0.61	0.10	0.84	0.74	0	0.56	0.56
	Sr	Inversion Energy	0.51	1.52	1.01	-0.14	0.62	0.76	-0.35	0.39	0.74
		Band Gap	0.18	0.82	0.64	0	0.62	0.62	0	0.39	0.39
	Ba	Inversion Energy	0.53	1.43	0.90	0	0.75	0.74	-0.18	0.55	0.73
		Band Gap	0	0.46	0.46	0	0.72	0.72	0	0.55	0.554

dispersion around this Dirac point is highly anisotropic: the velocity toward Γ is extremely small.

Fig. 3(b) shows the corresponding band structures for these strains. For 5% tensile strained $\text{Ca}_6\text{BiAsP}_2$ along Γ - Z, the two double spin-degenerate bands with $j_z = \frac{1}{2}$ and $j_z = \frac{3}{2}$ cross, producing a four-fold degenerate Dirac point which, as mentioned, is also orbitally degenerate due to the mirror symmetry with respect to the $x - y$ plane. Strain therefore interpolates between surface and bulk topological behavior in $\text{Ca}_6\text{BiAsP}_2$. The nearly flat band emerging from this Dirac point toward Γ may have implications for the transport properties.

Table I shows the band gap and inversion energy, including SOC, of selected double aPVs with and without the mBJ gap correction. Note that the inversion energy is defined as the energy difference between the “ext-S” and the valence band maximum. Some compounds show negative inversion energy; the band orderings have been inverted by SOC. These inversion energies are at least half the value of that added to the gap by the mBJ shift, in which case the band ordering is no longer inverted. The band gaps and the inversion energies show a range of values; the mBJ shifts are consistent across the $B = (\text{N}, \text{P}, \text{As})$ column. In general, compounds with nitrogen have a larger mBJ shift than the compounds with P or As.

VI. THERMOELECTRIC PROPERTIES

A. Formalism

The semiconducting band structures in these compounds suggest possible candidates for thermoelectric applications, with the possibly of learning more about the connection of thermoelectric properties to electronic structure.² Unlike the topological properties just discussed, which depend critically on positions in energy and dispersions in certain regions of the zone, the thermoelectric functions, viz. Seebeck coefficient S , power factor P , and figure of merit ZT depend almost entirely on the distribution of available states – the density of states $N(E)$. As commonly done, we treat the elastic scattering time τ as energy independent and isotropic, the latter being particularly good in cubic materials such as those we have treated here. For several properties τ cancels out.

The relations necessary to identify the origin of the

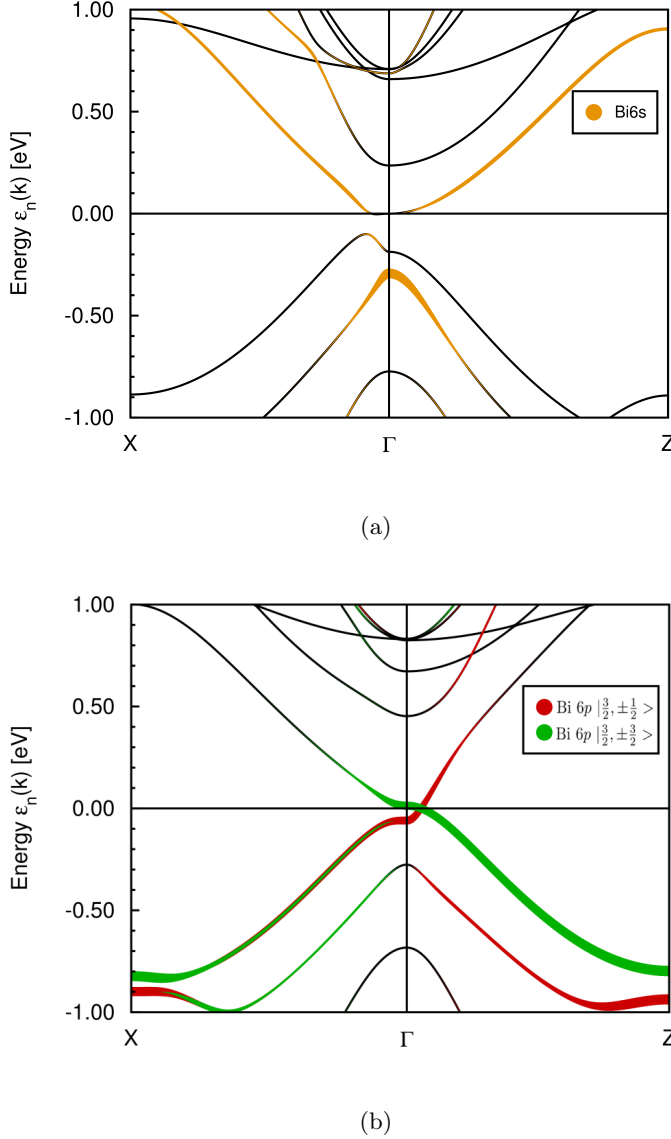


FIG. 3: GGA+mBJ band structure of uniaxial (001) strained $\text{Ca}_6\text{BiAsP}_2$, resulting in a topological insulator for 5% compressive strain (top panel) or Dirac semimetal for 5% tensile strain (bottom panel).

calculated behavior are the following.

$$\begin{aligned}
 S(T) &= \nu(T)/\sigma(T), \\
 \frac{\sigma(E)}{\tau} &= \frac{e^2}{3} N(E) v^2(E) \\
 \frac{\sigma(T)}{\tau} &= \int dE \frac{\sigma(E)}{\tau} \left[-\frac{df(E-\mu; T)}{dE} \right] \\
 \epsilon_F \frac{\nu(T)}{\tau} &= \frac{1}{eT} \int dE (E-\mu) \frac{\sigma(E, T)}{\tau} \left[-\frac{df(E-\mu; T)}{dE} \right] \\
 \frac{\kappa_e(T)}{\tau} &= \frac{1}{e^2 T} \int dE (E-\mu)^2 \frac{\sigma(E, T)}{\tau} \left[-\frac{df(E-\mu; T)}{dE} \right] \\
 P(T) &= S(T) \sigma(T) / \tau \\
 Z(T)T &= S^2(T) \frac{\sigma(T)/\tau}{\kappa_e/\tau}.
 \end{aligned} \tag{1}$$

κ_e is the electronic contribution to the thermal conductivity. The actual figure of merit Z includes a lattice contribution in the above equation as well as the electron one κ_e , so ZT as given above, and displayed below, is an ‘electronic figure of merit.’ $v^2(E)$ is the mean squared velocity averaged over the surfaces of constant energy E , and $f(E-\mu; T)$ is the Fermi-Dirac thermal distribution function. The Seebeck coefficient S is the ratio of the thermal and electric conductivity response functions, ν and σ respectively. The chemical potential $\mu(T)$ is determined at each temperature T to conserve particle number: $\mathcal{N} = \int N(E) f(E-\mu) dE$. Under the stated conditions, the quantities above are independent of τ . Note that the integrands in σ , ν , and κ_e involve increasingly higher powers of the carrier energy E with respect to μ , causing them to reflect more detail of the dispersion around the gap.

We caution that the lattice thermal conductivity is not included in our results. It will lower the value of the total ZT , but realistic calculations in line with these electronic contributions are challenging, and require additional algorithms and codes. The options, as outlined by Stackhouse and Stixrude,²³ are: the Green-Kubo thermal Greens function method, which at its most basic level a fully quantum-mechanical approach; non-equilibrium first principles molecular dynamics; transient non-equilibrium molecular dynamics, a version of the method just above requiring additional algorithms. Each of these requires special codes and is far beyond the scope of this paper and of most works evaluating the electronic contribution to ZT . Differences between oxides (where more work has been done) and nitrides will be mentioned in the Summary.

Another point is that the lattice thermal conductivity is dominated, especially at the lower temperature end, by acoustic modes. The compounds we propose have very heavy atoms (Bi or Sb) that will give acoustic modes low group velocities. The velocity enters the thermal conductivity as the square (see Stackhouse and Stixrude²³), hence as $1/M$ (mass). In addition, these heavy atoms reside in the large A site of the perovskite cell and may be expected to rattle (have large amplitude and be strongly

anharmonic), leading to a short relaxation time that will further reduce the lattice thermal conductivity. The correction to our ‘electronic figure of merit’ thus may be expected to be small.

The examples of the electronic thermoelectric behavior with temperature versus chemical potential μ (*i.e.* doping level) are plotted in Fig. 4 and will be discussed below. The “independent variable” μ in these plots account for both temperature and doping dependence. Temperature dependence is determined by the particle conservation mentioned just above. Doping dependence is treated in the rigid band approximation, which is reliable in itinerant systems in the low carrier density regime (where changes in band structure due to carriers is negligible). One then has the commonly quoted result that in the low temperature limit $S(T) \propto dN(E)/dE|_{E=\mu(0)}T$. Thus having $\mu(0)$ near a band edge or near other sharp structure in $N(E)$ leads to large values of $S(T)/T$.

B. Examples

Our discussion now will focus on two representative cases, the small gap (0.4 eV) semiconducting compound $\text{Ca}_6\text{BiAsN}_2$ (CBAN) and zero gap semiconductor $\text{Ca}_6\text{BiAsP}_2$ (CBAP). For both types of spectra, $\kappa_e(\mu)$ is not shown, as its behavior is simple: it has a minimum at the intrinsic chemical potential and rises quadratically to rather high doping levels, and the temperature dependence is unremarkable. The commonly studied electronic conductivity σ (also not shown) is a thermally broadened version of transport product $N(E)v^2(E)$ which is a much more slowly varying function of E than $N(E)$ and $v^2(E)$ separately.

The Seebeck coefficient shows the usual (for low doping) positive sign for hole doping $\mu < 0$ and negative sign for electron doping $\mu > 0$. The calculated value reaches nearly 2000 $\mu\text{V/K}$ at 100 K for CBAN, dropping to around 700 $\mu\text{V/K}$ at room temperature. In the more relevant coefficients, this high value is tempered by other energy-dependent factors. Unfortunately, the thermopower $P(T)$ does not make good use of the large values of $S(T)$ very near the gap, because the conductivity is low there. The thermopower becomes very low for μ within the gap, due to the extremely low conductivity there. Unlike the Seebeck coefficient which is nearly symmetric between electrons and holes, the thermopower reveals asymmetry, being nearly 40% lower for the holes at comparable doping levels.

For zero gapped CBAP, the Seebeck coefficient is an order of magnitude smaller than for CBAN, and the particle hole asymmetry is evident. This asymmetry of the effective masses is visible in Fig. 2. The conduction band minimum of CBAP at the Γ point has very small mass followed by higher velocities, due to the steep dip in conduction band at Γ also evident in Fig. 2. Since its valence band maximum remains free-electron-like, the Seebeck coefficient is asymmetric and somewhat shifted towards

negative chemical potential. The calculated electric conductivity and electronic thermal conductivity over relaxation time (not shown) of CBAN and CBAP are similar; they are further from the chemical potential and larger at higher temperature due to the enhancement of carrier concentration.

The thermopower and figure of merit ZT quantify the potential efficiency in thermoelectric applications. The power factor of CBAN shows two peaks around $\mu = 0$, while that of CBAP shows a higher peak at positive chemical potential, indicating that better thermoelectric properties can be realized by electron doping. With rising temperature, the value of the power increases by five times and eight times for CBAN and CBAP respectively, from room temperature to 800 K.

At 100 K, ZT of CBAN is calculated to be unity for low doping levels of either sign. This dimensionless thermoelectric device efficiency decreases slowly with rising temperature, dropping by only 5% at room temperature. This small decrease indicates that this material has the potential to produce thermoelectric power effectively at low temperature. For zero gap CBAP, the value is half that of the small gap semiconductor. Nevertheless, these values are among the highest found in the literature,^{24,25} including these promising thermoelectric double perovskites²⁶⁻³⁰. Our results indicate that these pnictide-based double antiperovskites have the potential to be competitive thermoelectric materials.

VII. SUMMARY

The topological characteristics and thermoelectric properties of representative pnictide-based double antiperovskites have been studied. Doubling the perovskite structure offers a larger bulk insulating gap than single perovskite provides, plus they are more likely to be inverted by SOC. Based on the GGA exchange-correlation functional, uniaxial compressive strain opens up an energy gap at the Γ point producing a topological insulator with a large bulk band gap. Tensile strain along z direction, on the other hand, gives a Dirac semimetal with Dirac band crossing along $\Gamma - Z$. However, an uncertainty remains whether these topological materials can be realized, as the corrections to the band energy calculation with mBJ potential suggest trivial insulators.

Nonetheless, they are potential candidates for thermoelectric applications due to the high values of Seebeck coefficient, thermoelectric power and figure of merit.

VIII. ACKNOWLEDGMENTS

W.F.G. was supported by NSF Grant DMR 1534719, while W.E.P. had support from DOE grant DE-FG02-04ER46111.

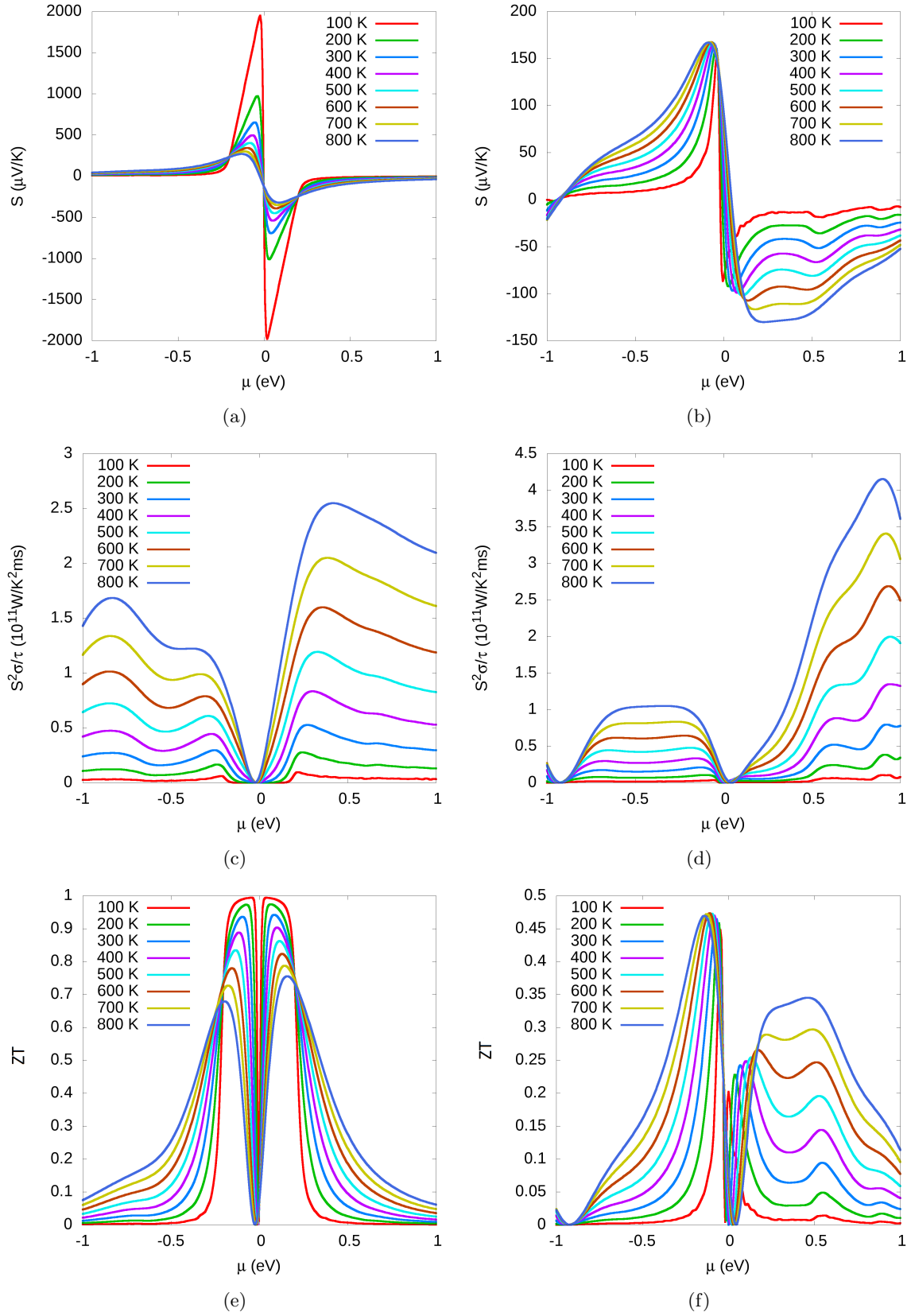


FIG. 4: The Seebeck coefficient (top panels), thermopower (middle panels), and figure of merit ZT (lower panels) of $\text{Ca}_6\text{BiAsN}_2$ (left column) with small gap and $\text{Ca}_6\text{BiAsP}_2$ (right column) with zero gap, versus chemical potential, in the temperature range 100K – 800K.

IX. BIBLIOGRAPHY

- ¹ C.L. Kane and E. J. Mele, Z_2 Topological Order and the Quantum Spin Hall Effect, *Phys. Rev. Lett.* **95**, 146802 (2005).
- ² H. Shi, D. Parker, M-H. Du, and D. J. Singh, Connecting Thermoelectric Performance and Topological-Insulator Behavior: Bi_2Te_3 and $\text{Bi}_2\text{Te}_2\text{Se}$ from First Principles, *Phys. Rev. Applied* **3**, 014004 (2015).
- ³ Devender, P. Gehring, A. Gaul, A. Hoyer, K. Vaklinova, R. J. Mmehtha, M. Burghard, T. Borca-Tasciuc, D. J. Singh, K. Kern, and G. Ramanath, Harnessing Topological Band Effects in Bismuth Telluride Selenide for Large Enhancements in Thermoelectric Properties through Isovalent Doping, *Adv. Mater.* **28**, 6436 (2016).
- ⁴ H. Zhang, C. X. Liu, X. L. Qi, X. Dai, Z. Fang, and S. C. Zhang, Topological insulators in Bi_2Se_3 , Bi_2Te_3 and Sb_2Te_3 with a single Dirac cone on the surface, *Nat. Phys.* **5**, 438 (2009).
- ⁵ W. Zhang, R. Yu, H. J. Zhang, X. Dai, and Z. Fang, First-principles studies of the three-dimensional strong topological insulators Bi_2Te_3 , Bi_2Se_3 and Sb_2Te_3 , *New J. Phys.* **12**, 065013 (2010).
- ⁶ O. V. Yazyev, J. E. Moore, and S. G. Louie, Spin polarization and transport of surface states in the topological insulators Bi_2Se_3 and Bi_2Te_3 from first principles, *Phys. Rev. Lett.* **105**, 266806 (2010).
- ⁷ H. Jin, S. H. Rhim, J. Im and A. J. Freeman, Topological oxide insulator in cubic perovskite structure, *Sci. Rep.* **3**, 1651 (2013).
- ⁸ M. Yang and R. N. Wang, Topological insulator in tellurium-based perovskites, *Int. J. Mod. Phys. B* **29**, 1550073 (2015).
- ⁹ H. Jin, J. Im, and A. J. Freeman, Topological insulator phase in halide perovskite structures, *Phys. Rev. B* **86**, 121102 (2012).
- ¹⁰ Y. Sun, X. Q. Chen, S. Yunoki, D. Li and Y. Li, New family of three-dimensional topological insulators with antiperovskite structure, *Phys. Rev. Lett.* **105**, 216406 (2010).
- ¹¹ T. H. Hsieh, J. Liu, and L. Fu, Topological crystalline insulators and Dirac octets in antiperovskites, *Phys. Rev. B* **90**, 081112 (2014).
- ¹² M. Bilal, Saifullah, M. Shafiq, B. Khan, H. A. R. Aliabad, S. J. Asadabadid, R. Ahmad and I. Ahmad, Antiperovskite compounds SbNSr_3 and BiNSr_3 : Potential candidates for thermoelectric renewable energy generators, *Phys. Lett. A* **379**, 2067 (2015).
- ¹³ S. T. Pi, H. Wang, J. Kim, R. Wu, Y. K. Wang and C. K. Lu, New Class of 3D Topological Insulator in Double Perovskite, *J. Phys. Chem. Lett.* **8**, 332 (2017).
- ¹⁴ P. H. Lee, J. Zhou, S. T. Pi and Y. K. Wang, Topological insulators double perovskites: A_2TePoO_6 ($\text{A}=\text{Ca}, \text{Sr}, \text{Ba}$), *J. Appl. Phys.* **122**, 224902 (2017).
- ¹⁵ W. F. Goh and W. E. Pickett, Survey of the class of isovalent antiperovskite alkaline-earth pnictide compounds, *Phys. Rev. B* **97**, 035202 (2018).
- ¹⁶ K. Koepernik and H. Eschrig, Full-potential nonorthogonal local-orbital minimum-basis band-structure scheme, *Phys. Rev. B* **59**, 1743 (1999).
- ¹⁷ J. P. Perdew, K. Burke and M. Ernzerhof, Generalized Gradient Approximation Made Simple, *Phys. Rev. Lett.* **77**, 3865 (1996).
- ¹⁸ P. Blaha, K. Schwarz, G. K. H. Madsen, D. Kvasnicka and J. Luitz, *WIEN2K: An Augmented Plane Wave + Local Orbitals Program for Calculating Crystal Properties* (Techn. Universität Wien, 2001).
- ¹⁹ G. K. H. Madsen and D. J. Singh, BoltzTraP. A code for calculating band-structure dependent quantities, *Comput. Phys. Commun.* **175**, 67 (2006).
- ²⁰ A. D. Becke and E. R. Johnson, A simple effective potential for exchange, *J. Chem. Phys.* **124**, 221101 (2006).
- ²¹ F. Tran, P. Blaha and K. Schwarz, Band gap calculations with Becke-Johnson exchange potential, *J. Phys.: Condens. Matter.* **19**, 196208 (2007).
- ²² F. Tran and P. Blaha, Accurate Band Gaps of Semiconductors and Insulators with a Semilocal Exchange-Correlation Potential, *Phys. Rev. Lett.* **102**, 226401 (2009).
- ²³ S. Stackhouse and L. Stixrude, Theoretical Methods for Calculating the Lattice Thermal Conductivity of Minerals, *Rev. in Mineralogy and Geochemistry* **71**, 253 (2010).
- ²⁴ J. Li, G. Yang, Y. Yang, H. Ma, Q. Zhang, Z. Zhang, W. Fang, F. Yin and J. Li, Electronic and thermoelectric properties of nonmagnetic inverse Heusler semiconductors Sc_2FeSi and Sc_2FeGe , *J. Magn. Magn. Mater.* **442**, 371 (2017).
- ²⁵ K. C. Bhamu and C. S. Praveen, Thermoelectric properties of 2H-CuGaO_2 for device applications: A first principle TB-mBJ potential study, *J. Solid State Chem.* **256**, 101 (2017).
- ²⁶ M. H. Aguirre, D. Logvinovich, L. Bocher, R. Robert, S. G. Ebbinghaus and A. Weidenkaff, High-temperature thermoelectric properties of Sr_2RuYO_6 and $\text{Sr}_2\text{RuErO}_6$ double perovskites influenced by structure and microstructure, *Acta Mater.* **57**, 108 (2009).
- ²⁷ O. Sahnoun, H. Bouhani-Benziane, M. Sahnoun and M. Driz, Magnetic and thermoelectric properties of ordered double perovskite $\text{Ba}_2\text{FeMoO}_6$, *J. Alloys Compd.* **714**, 704 (2017).
- ²⁸ R. Takahashi, R. Okazaki, Y. Yasui, I. Terasaki, T. Sudo, H. Nakao, Y. Yamasaki, J. Okamoto, Y. Murakami and Y. Kitajima, High-temperature thermoelectric properties of the double-perovskite ruthenium oxide ($\text{Sr}_{1-x}\text{La}_x$) $_2\text{ErRuO}_6$, *J. Appl. Phys.* **112**, 073714 (2012).
- ²⁹ P. Roy, V. Waghmare and T. Maiti, Environmentally friendly $\text{Ba}_x\text{Sr}_{2-x}\text{TiFeO}_6$ double perovskite with enhanced thermopower for high temperature thermoelectric power generation, *RSC Adv.* **6**, 54636 (2016).
- ³⁰ P. Villar Arribi, P. García-Fernández, and J. Junquera and V. Pardo, Efficient thermoelectric materials using nonmagnetic double perovskites with d^0/d^6 band filling, *Phys. Rev. B* **94**, 035124 (2016).